Impact of Reference Center Choice on Adaptive Optics Imaging Cone Mosaic Analysis

Danial Roshandel,[1,2] Danuta M. Sampson,[3] David A. Mackey,[1] and Fred K. Chen[1,4,5]

[1]Centre for Ophthalmology and Visual Science (incorporating Lions Eye Institute), The University of Western Australia, Perth, Western Australia, Australia
[2]Ocular Tissue Engineering Laboratory, Lions Eye Institute, Nedlands, Western Australia, Australia
[3]Surrey Biophotonics, Centre for Vision, Speech and Signal Processing and School of Biosciences and Medicine, The University of Surrey, Guildford, United Kingdom
[4]Ophthalmology, Department of Surgery, University of Melbourne, Melbourne, Victoria, Australia
[5]Centre for Eye Research Australia, Royal Victorian Eye and Ear Hospital, Melbourne, Victoria, Australia

Correspondence: Fred K. Chen, Lions Eye Institute, 2 Verdun Street, Nedlands WA 6009, Australia; fredchen@lei.org.au.

Received: October 10, 2021
Accepted: March 30, 2022
Published: April 21, 2022

Citation: Roshandel D, Sampson DM, Mackey DA, Chen FK. Impact of reference center choice on adaptive optics imaging cone mosaic analysis. *Invest Ophthalmol Vis Sci.* 2022;63(4):12. https://doi.org/10.1167/iovs.63.4.12

Purpose. Foveal center marking is a key step in retinal image analysis. We investigated the discordance between the adaptive optics (AO) montage center (AMC) and the foveal pit center (FPC) and its implications for cone mosaic analysis using a commercial flood-illumination AO camera.

Methods. Thirty eyes of 30 individuals (including 15 healthy and 15 patients with rod–cone dystrophy) were included. Spectral-domain optical coherence tomography was used to determine the FPC, and flood-illumination AO imaging was performed with overlapping image frames to create an AO montage. The AMC was determined by averaging the (0,0) coordinates in the four paracentral overlapping AO image frames. Cone mosaic measurements at various retinal eccentricities were compared between corresponding retinal loci relative to the AMC or FPC.

Results. AMCs were located temporally to the FPCs in 14 of 15 eyes in both groups. The average AMC–FPC discordance was 0.85° among healthy controls and 0.33° among patients with rod-cone dystrophy ($P < 0.05$). The distance of the AMC from the FPC was a significant determinant of the cone density (β estimate = 218 cells/deg^2/deg; 95% confidence interval [CI], 107–330; $P < 0.001$) and inter-cone distance (β estimate = 0.28 arcmin/deg; 95% CI, 0.15–0.40; $P < 0.001$), after adjustment for age, sex, axial length, spherical equivalent, eccentricity, and disease status.

Conclusions. There is a marked mismatch between the AMC and FPC in healthy eyes that may be modified by disease process such as rod–cone dystrophy. We recommend users of AO imaging systems carefully align the AO montage with a foveal anatomical landmark, such as the FPC, to ensure precise and reproducible localization of the eccentricities and regions of interest for cone mosaic analysis.

Keywords: adaptive optics imaging, fovea, foveal pit center, cone mosaic, rod–cone dystrophy

Accurate localization of the region of interest (ROI) is a crucial step in retinal image analysis. The foveal pit center (FPC) as determined using optical coherence tomography (OCT) has been used widely as the reference point for assigning ROIs within the macula.[1] However, most en face imaging modalities do not provide landmarks to allow precise localization of the FPC. In the healthy eye, it is often incorrectly assumed that the retinal locus used by the patient for staring at the internal fixation target to maintain eye stability during the test coincides with the FPC. It is well recognized that there is a physiologic instability in the eye position, governed by fixational eye movements, during retinal imaging or microperimetry characterized by a series of slow drifts and microsaccades.[2] Several methods have been used to define the preferred fixation locus, also known as the preferred retinal locus (PRL), such as the centroid of the region encompassing 95% of fixation points used during a fixation task quantified by the bivariate contour ellipse area (BCEA).[3] Given that the greatest diameter of the BCEA used during microperimetry can vary from 0.6° to 1.8° in healthy controls across different age groups,[4] it is not surprising that there is a potential for significant disparity between the PRL and FPC.[5] In addition, the position of the fixation point and fixation behavior might be affected by the size, shape, luminance, or color of the internal fixation target.[6–8] Hence, relying on the PRL during retinal imaging instead of the FPC for defining retinal eccentricity may result in inaccurate measurement at specific ROIs.

Adaptive optics (AO) imaging is a powerful tool for studying photoreceptor packing and distribution in the human retina. Cone density and spacing derived from AO scanning laser ophthalmoscopy (AOSLO)[9] and AO flood-illumination

ophthalmoscopy[10] are comparable to histologic findings.[10] Distance from the FPC has been the strongest determinant of cone density and spacing in normal eyes.[11] In addition, cones are more densely packed along the horizontal meridian compared to the vertical meridian.[10] Definitions used to define the foveal center include the fixation point,[12,13] location of peak cone density,[14] center of the iso-density ellipse (the ellipse that connects locations with the same cone density),[10,15] and anatomical center of the foveal pit.[16] AO cameras, including the rtx1 (Imagine Eyes, Orsay, France), often select the first retinal fixation locus used during an AO imaging session as the reference coordinate (x,y) of (0,0) for assigning retinal eccentricity within the single image frame. We recently demonstrated that foveal centers determined by co-registration between spectral-domain optical coherence tomography (SD-OCT) B-scan and infrared (IR) fundus images may not coincide with the (0,0) locus of the AO image frame acquired on the rtx1 device in healthy individuals.[17] This disparity may result in inaccurate and inconsistent localization of the ROI and cone mosaic measurements using the coordinates provided by the device. Given that clinical trials (www.ClinicalTrials.gov) are already using AO imaging to study the natural history of cone photoreceptor degeneration such as rod–cone dystrophy (RCD; e.g. NCT03349242, NCT00254605, and NCT01866371), there is an unmet clinical need to examine the disparity in location between the FPC and the AO montage center (AMC) and its impact on AO image analysis in future clinical trials using the commercial AO imaging device.

In this study, we analyzed the discordance between the AMC and the FPC in healthy eyes and eyes with RCD and its impact on cone mosaic analysis using a commercial AO flood-illumination ophthalmoscopy retinal camera and its integrated analysis software.

Methods

Participants

Thirty subjects (16 females) were enrolled, including 15 healthy controls and 15 patients with RCD (Supplementary Table S1). The mean age was 43 years (SD, 16; range, 18–65). Anonymized images from healthy subjects and patients with RCD were selected from participants enrolled in two prospective studies: the Distortion Scotoma Assessment (DSA) study and the Western Australian Retinal Degeneration (WARD) study. The study protocols for both studies were approved by the Human Ethics Committee of the Office of Research Enterprise, The University of Western Australia (RA/4/1/7226, RA/4/1/7916, 2021/ET000151, and 2021/ET000895) and adhered to the tenets of the Declaration of Helsinki. Informed written consent was obtained from all participants.

Subjects from the DSA and WARD studies with AO images were included if they were 18 years of age or older and had stable foveal fixation (i.e., no apparent eccentric fixation and/or nystagmus on clinical examination). Patients with best-corrected visual acuity (BCVA) equal to or better than 20/40 and clinical and electrophysiological diagnosis of RCD were enrolled. Inclusion criteria for healthy subjects were normal ocular examination and no history of ocular disease. Exclusion criteria for both groups were history of ocular surgery, significant cataract or other media opacity, nystagmus, significant cystoid macular edema or epiretinal membrane, and use of systemic medications with known photoreceptor toxicity. Ocular health and diagnosis of RCD were confirmed by an experienced inherited retinal disease specialist (author FKC).

Clinical Evaluations and Imaging Protocols

All subjects underwent complete ophthalmic examinations, including BCVA, slit-lamp bio-microscopy with Goldmann applanation tonometry (Haag-Streit AG, Koeniz, Switzerland), and dilated fundus examination. Autorefraction (ARK-1 Autorefractor/Keratometer; Nidek, Gamagori, Japan) and optical biometry (IOL Master; Carl Zeiss Meditec, Inc., Dublin, CA, USA) were performed to measure the spherical equivalent (SE) and the axial length (AL), respectively.

Macular integrity assessment (MAIA) microperimetry (MAIA microperimeter; CenterVue, Padova, Italy) was performed using a 4-2 staircase strategy and 10-2 grid pattern. The test was performed with pupils fully dilated, after the patient accustomed to the darkness of the testing room for 5 minutes and before retinal imaging was performed. Mean sensitivity and fixation parameters including the BCEA 63%, BCEA 95%, P1, and P2 were recorded. P1 and P2 represent the percentage of fixation points that fall within the central 1° and 2°, respectively. Fixation was considered stable if P1 > 75% and relatively stable if P1 < 75% and P2 > 75%.

For SD-OCT (SPECTRALIS OCT; Heidelberg Engineering, Heidelberg, Germany), patients were instructed to fixate on the internal fixation target while foveal-centered macular volume scans (30° × 25° scan field, 61 horizontal B-scans separated by 130 µm, equivalent to approximately 0.4°) were taken. Also, near-infrared and short-wavelength fundus autofluorescence imaging (Heidelberg Retina Angiograph 2, HRA2; Heidelberg Engineering) were performed in the patient group to detect the macular hyperautofluorescent ring. The residual ellipsoid zone span and area of the hyperautofluorescent ring in patients with RCD were measured using HEYEX version 1.9.14.0 (Heidelberg Engineering) as described before.[18] Briefly, the ellipsoid zone span was measured on foveal B-scans as the distance between the nasal and temporal endings of the ellipsoid zone. The outer border of the hyperautofluorescent ring was demarcated, and its area was reported.

AO imaging using the rtx1 was performed with pupil dilation under a dim light condition and without dark adaptation. The photoreceptor module of manufacturer software (AO Image 3.0) was used for image acquisition. The focus plane was set from +40 µm to +100 µm (corresponding to 40–100 µm above the retinal pigment epithelium [RPE]). Subjects were instructed to fixate on the internal cross-hair fixation target, and the fixation was monitored by the operator using the live pupil centration view provided in the software (Supplementary Fig. S1). Alignment between the fixation target and the camera indicator was confirmed by experienced observers throughout the experiment. In each acquisition, 40 images were captured during 4 seconds (10 frames per second), which were aligned and averaged using the internal software to increase the signal-to-noise ratio. Twelve 4° × 4° image frames with a 2° × 4° region overlap with the adjacent frame, covering the central 5°, were taken from each eye. The fixation coordinates (x,y) for the 12 image frames were as follows: 1N, +1; 1N, –1; 1T, +1; 1T, –1; 3N, +1; 3N, –1; 3T, +1; 3T, –1; 1N, +3; 1N, –3; 1T, +3; and 1T, –3, where N is nasal and T is temporal for the x-axis or the horizontal coordinate. Individual AO images were stitched and merged using the MosaicJ plugin for

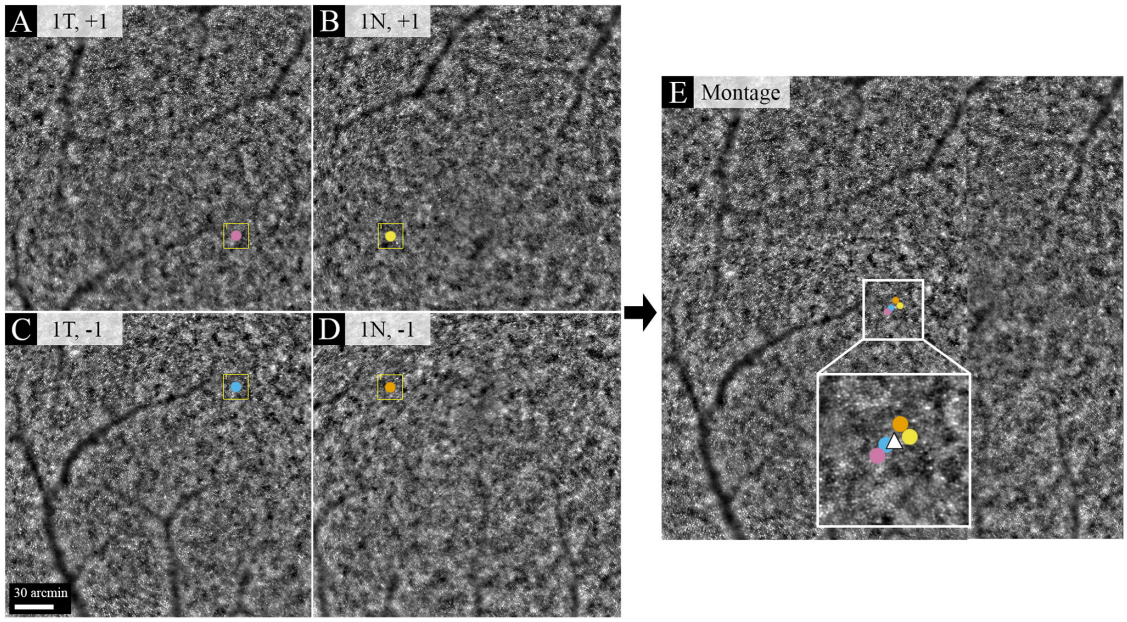

Figure 1. (**A–D**) The location of the (0,0) coordinate was marked on four overlapping paracentral image frames by the AODetect software. (**E**) The image frames were superimposed, and the average center of the four markings was assigned as the AMC (*white triangle*).

ImageJ (National Institutes of Health, Bethesda, MD, USA) to create a widefield montage.

Assigning the AMC and FPC

To determine the AMC, first the (0,0) coordinate of each image frame was identified and marked (as a square box) by the onboard software in the four central AO images that incorporated the foveal center in the image frame (Figs. 1A–1D). These four central image frames were inspected, and the eye was excluded if there was a notable (>0.2°) disparity in the (0,0) locus among any of the four image frames after alignment and superimposition using Adobe Photoshop CC 2015 (Adobe Systems, Inc., San Jose, CA, USA). The center of the four (0,0) markings was found on the AO montage, and the horizontal and vertical average position of these four loci was assigned as the AMC (Fig. 1E).

To locate the FPC, the foveal-centered SD-OCT B-scan and the accompanying IR image were used to mark the FPC along the vertical meridian (Fig. 2A). The horizontal foveal center was defined as the center of the retinal region without inner retinal layers (Fig. 2B), and the central point was found and marked on the IR fundus image using the manufacturer's software (HEYEX 1.9.14.0; Heidelberg Engineering).

The AO montage with marked AMC was superimposed on the FPC-marked IR image by matching the large vessels using Adobe Photoshop. The FPC was marked on the AO montage that already had the AMC marked (Fig. 3). Alignments were confirmed by a senior author (FKC) who was masked to the diagnoses and adjusted if required. It has been shown that montage creation does not affect the coordinates of the image frame center (less than 4% displacement),[15] and cone density is comparable using montage-derived and gaze-directed coordinates.[16] The distance between the AMC and the FPC on the *x*- and *y*-axes was measured in pixels and converted to angular units using axial length (Fig. 3). The rotation of the AO montage in relation to the IR fundus image during the alignment process was also

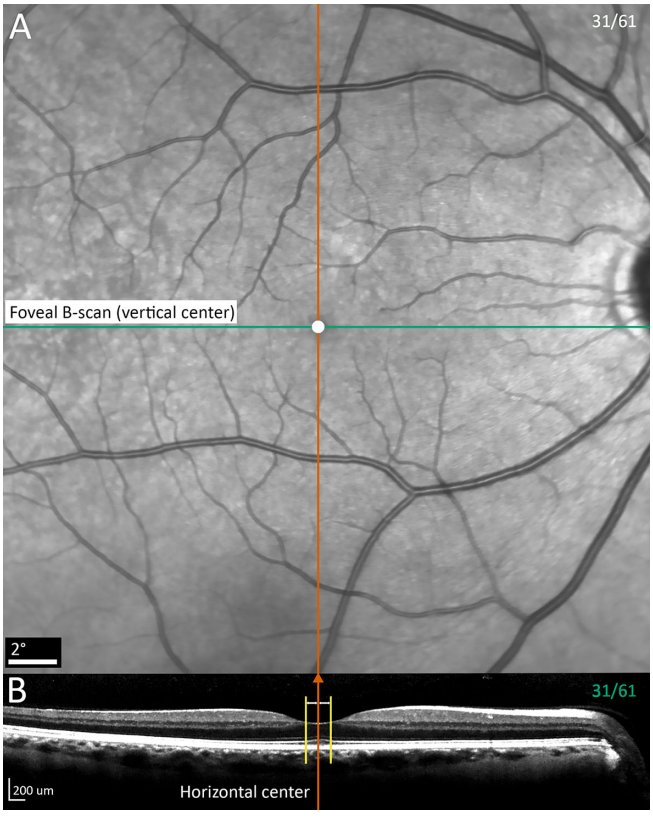

Figure 2. The FPC was localized and marked on the co-registered retinal infrared image and horizontal foveal B-scan. (**A**) The foveal-centered B-scan (*green horizontal line*) was used to determine the vertical center. (**B**) The inner retinal-free area (delineated by the *vertical yellow lines*) was divided into two equal parts (*white lines*), and its center (*vertical orange line*) was used to determine the horizontal center. The intersection between the vertical and the horizontal central lines is marked as the FPC on the en face image (*white dot* in panel **A**).

Investigative Ophthalmology & Visual Science

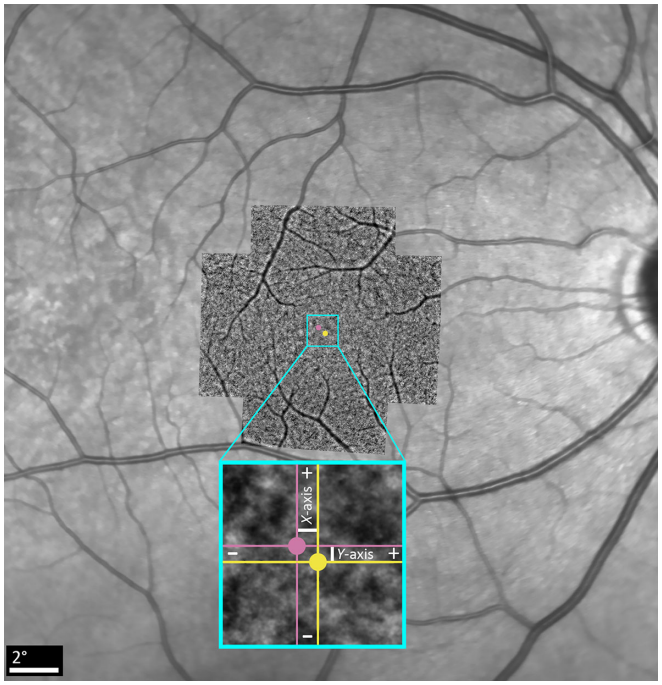

Figure 3. The AO montage with marked AMC (*pink*) was superimposed on the FPC-marked (*yellow*) infrared retinal image. Horizontal and vertical distances between the AMC and the FPC were measured and reported.

measured. To examine the disparity between the AMC and the PRL derived from MAIA 10-2 microperimetry, MAIA scanning laser ophthalmoscopy (SLO) images and fundus sensitivity maps were superimposed on the AMC-marked AO montage.

Cone Mosaic Analysis

Commercial software (AODetect 3.0; Imagine Eyes) was used for cone detection, segmentation, and packing analysis. Analyses were performed at 2° and 4° eccentricities in four directions (i.e., nasal, superior, temporal, and inferior), relative to both the AMC and the FPC separately (Fig. 4). The total number of images obtained at the 2° and 4° locations for each eye and along each meridian were 4 and 2 images, respectively. Image quality was assessed by an author (DR) based on clarity of the cone mosaic. ROIs with a clearly visible cone mosaic were included in the final image analysis, and those with missing cone mosaics within any portion of the ROI were excluded. Cones were marked automatically in an 80 × 80-µm window and adjusted manually by an experienced AO grader (author DR). Cone mosaic parameters including cone density and inter-cone distance were calculated and reported in linear units (cells/mm^2 and µm, respectively) and angular units (cells/deg^2 and arcmin, respectively) (Supplementary Fig. S2). For each ROI, the sampling window was placed at the closest location that was free from large vessels. If the ROI was captured by two or more overlapping image frames, the image frame with the highest image quality (as determined by author DR) was selected, and all measurements were performed on the same image frame. The angular and linear cone density and inter-cone distance values were recorded and used for subsequent statistical analyses.

Statistical Analysis

Data were recorded in SPSS Statistics 23 (IBM, Inc., Chicago, IL, USA), and appropriate statistics were applied after testing for normality. Visual acuities were converted to logarithm of minimum angle of resolution (logMAR) units. Only right-eye data were used for statistical analysis. The Shapiro–Wilk test for normality showed non-normal distribution of all

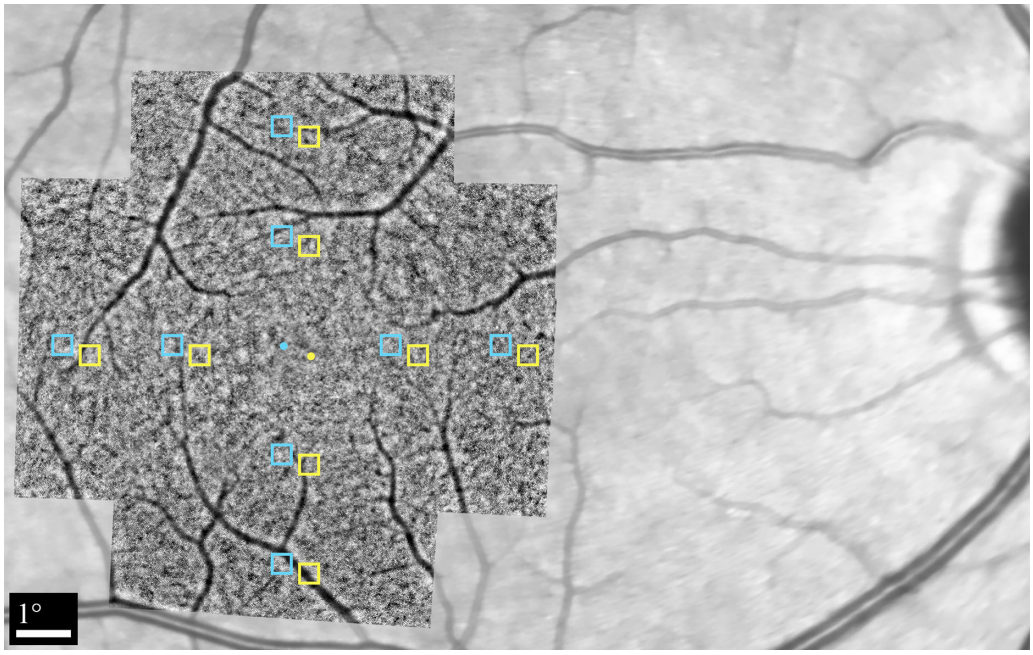

Figure 4. The AMC (*blue dot*) and FPC (*yellow dot*) were used to localize corresponding regions of interest (*squares*) along the four retinal meridians.

Investigative Ophthalmology & Visual Science

variables; hence, nonparametric tests were used for analyzing mean differences between independent and related samples. Specifically, the Mann–Whitney *U*-test was used to compare mean baseline characteristics and foveal discordance between the control and patient groups, and the Wilcoxon signed-rank test was used to compare mean cone density and inter-cone distance between meridians and eccentricities using the AMC versus FPC in the same eyes. In addition, general linear model multiple regression analysis was performed to assess the contribution of different factors to the AMC–FPC discordance and cone mosaic measurements. $P < 0.05$ was considered statistically significant, with Bonferroni adjustment for multiple statistical comparisons.

Results

There was no significant difference in the mean fixation parameters between the patient and control groups. Mean BCVA and mean sensitivity were significantly higher in the control group compared with the patient group (Table 1). Ellipsoid zone defects and hyperautofluorescent rings were detected in 12 and 11 RCD patients, respectively. The mean residual ellipsoid zone span and hyperautofluorescent ring area in the patient group were 2838 µm (SD, 1436; range, 1200–6608) and 5.4 mm^2 (SD, 2.6; range, 1.3–9.6), respectively.

Discordance Between the AMC and the FPC

None of the imaged eyes showed > 0.2° disparity in the (0,0) coordinate among the four central image frames. The AMC was located temporally to the FPC in 14 of 15 cases in both groups (Table 2). The mean horizontal disparities between the AMC and the FPC in the control and patient groups were 0.85° (SD, 0.58°; range, 0°–1.54°) and 0.33° (SD, 0.30°; range, 0.34°–1.09°), respectively ($P = 0.03$). The temporal displacement of the AMC was greater than 1.0° in eight of 15 controls and in only one of 15 patients (Table 2, Fig. 5). Using multivariate regression analysis, disease status (healthy vs. disease) was the only factor that significantly contributed to the horizontal AMC–FPC disparity (β estimate = 0.98°; 95% confidence interval [CI], 0.20–1.76; $P = 0.017$) and overall AMC–FPC disparity (β estimate = 1.00°; 95% CI, 0.30–1.70; $P = 0.008$). There was no significant relationship between the other factors, such as age, sex, AL, SE, BCVA, mean sensitivity, and fixation parameters and foveal disparity. Also, rotational and vertical AMC–FPC disparities were not related to any of the factors, including disease status (Table 3). In

Table 1. Demographic and Clinical Characteristics of Participants

Group	ID	Sex	Age (y)	SE (D)	AL (mm)	BCEA (deg^2) 63%; 95%	P1; P2 (%)	MS (dB)	BCVA (logMAR)
Healthy									
	1	M	21	–4.75	25.4	0.3; 1.0	99; 100	30.0	–0.08
	2	M	22	0.0	23.75	0.1; 0.3	100; 100	29.1	–0.02
	3	F	25	–3.25	24.88	3.4; 10.1	82; 94	25.1	0.06
	4	M	29	–0.50	23.40	0.4; 1.2	98; 100	26.1	–0.18
	5	M	44	0.125	25.01	0.8; 2.3	94; 98	29.2	–0.20
	6	M	52	–0.125	23.99	1.0; 2.9	93; 99	26.0	–0.20
	7	F	53	1.25	23.95	1.0; 2.9	93; 100	28.8	–0.16
	8	F	54	0.0	24.45	1.7; 5.2	86; 98	28.6	–0.16
	9	F	54	0.50	24.80	1.3; 4.0	91; 97	24.5	–0.02
	10	M	58	0.875	23.63	0.4; 1.2	99; 100	26.1	–0.10
	11	M	58	–3.25	23.99	0.4; 1.2	99; 100	28.5	–0.06
	12	F	62	–1.375	23.83	2.7; 8.0	79; 95	27.3	–0.08
	13	F	62	0.75	23.16	0.3; 0.8	99; 100	28.8	–0.20
	14	F	64	–0.25	23.08	2.9; 8.8	77; 94	24.6	–0.10
	15	F	65	2.00	23.09	0.6; 1.7	97; 100	29.3	–0.18
	Mean (SD)		48 (16)	–0.53 (1.87)	24.03 (0.73)	1.2 (1.2); 3.4 (3.2)	92 (8); 98 (2)	27.5 (1.9)	–0.12 (0.08)
Disease									
	16	M	18	0.25	23.48	0.6; 1.9	96; 99	11.8	0.00
	17	M	19	3.25	22.54	2.8; 8.3	80; 94	29.8	0.04
	18	M	21	–1.25	24.33	0.5; 1.4	98; 100	26.1	0.12
	19	M	24	–0.50	23.80	0.7; 2.0	97; 99	12.4	0.32
	20	M	24	–1.50	23.57	0.6; 1.9	96; 100	2.3	0.20
	21	M	30	–2.25	23.45	0.1; 0.3	100; 100	7.0	–0.02
	22	F	37	–0.25	22.31	0.2; 0.6	100; 100	23.5	–0.08
	23	F	38	–0.50	22.85	2.3; 6.9	89; 96	15.5	0.00
	24	F	40	–0.75	22.56	6.7; 20.2	74; 89	NA	0.10
	25	M	40	1.00	22.50	0.7; 2.1	98; 100	12.4	0.02
	26	F	43	–8.25	27.71	0.4; 1.1	100; 100	13.8	–0.06
	27	F	47	0.75	22.46	0.2; 0.6	99; 100	16.2	0.02
	28	F	56	–0.50	23.80	2.1; 6.3	85; 96	13.6	0.00
	29	F	57	3.00	21.84	19.5; 58.5	4; 75	0.6	0.10
	30	F	62	1.75	22.68	0.3; 0.9	99; 100	25.7	–0.02
	Mean (SD)		37* (14)	–0.38 (2.68)	23.32* (1.40)	2.5 (5.0); 7.5 (15.0)	88 (25); 99 (7)	15.1* (8.7)	0.05* (0.10)

BCEA 63% and 95%, area of the bivariate contour ellipse encompassing 63% and 95% of the fixation points, respectively; P1 and P2, percentage of fixation points within the central 1° and 2°, respectively; MS, mean sensitivity; M, male; F, female.

* Significant compared with control group, $P < 0.05$.

Investigative Ophthalmology & Visual Science

Table 2. Misalignment Between the AMC and FPC

Group	ID	*x*-Axis (°)*	*y*-Axis (°)*	Distance (°)†	Rotation (°)‡
Healthy	1	–1.16	0.00	1.16	0.33
	2	–1.39	0.12	1.41	0.13
	3	–1.51	0.02	1.51	0.90
	4	–0.39	–0.14	0.41	1.37
	5	–0.11	0.09	0.12	0.68
	6	–1.54	0.19	1.57	–1.28
	7	–1.21	–0.10	1.22	–0.30
	8	–1.38	0.18	1.42	0.70
	9	0.00	0.58	0.34	–0.50
	10	–0.19	0.86	0.93	1.10
	11	–0.47	.032	0.57	–0.50
	12	–0.25	0.12	0.26	1.97
	13	–1.43	0.01	1.43	–0.40
	14	–0.54	–0.90	1.35	2.35
	15	–1.25	–0.01	1.25	0.00
	Mean (SD)	–0.85 (0.58)	0.09 (0.38)	1.00 (0.51)	0.44 (1.00)
Disease	16	–0.46	–0.01	0.46	0.30
	17	–0.37	0.45	0.57	1.20
	18	–0.26	–0.18	0.30	–0.37
	19	–0.58	0.01	0.58	0.55
	20	–0.21	0.78	0.82	–0.96
	21	–1.09	0.23	1.00	0.30
	22	0.34	–0.15	0.37	0.17
	23	–0.25	0.41	0.42	0.41
	24	–0.41	0.51	0.67	–4.10
	25	–0.31	–0.02	0.31	–1.38
	26	–0.21	0.32	0.31	1.88
	27	–0.52	0.28	0.60	2.36
	28	–0.27	0.14	0.29	0.00
	29	–0.19	0.20	0.23	1.30
	30	–0.17	–0.01	0.17	0.92
	Mean (SD)	–0.33§ (0.30)	0.20 (0.27)	0.48§ (0.26)	0.17 (1.54)

* Negative values indicate temporal (*x*-axis) and inferior (*y*-axis) displacement of the AMC.

† Absolute distance between the AMC and the FPC.

‡ Rotation of the AO montage in relation to the infrared fundus image. Negative values indicate counterclockwise rotation; positive values indicate clockwise rotation.

§ Significant compared with the control group, $P < 0.05$.

addition, there was no significant correlation between the AMC–FPC offset and age, sex, fixation parameters, BCVA, or mean sensitivity within each group. BCVA in controls with AMC–FPC offset greater than 1° was not statistically different from those with an offset less than 1°. Ellipsoid zone span and hyperautofluorescent ring area were not correlated with horizontal, vertical, or overall AMC–FPC discordance in the patient group.

Accurate alignment of the MAIA SLO fundus image with the AO montage was possible in five healthy controls. MAIA-derived PRLs were located 0.08° to 0.19° (mean, 0.15°; SD, 0.04°) away from the FPC, which was deviated temporally in four subjects and nasally in one subject (Supplementary Table S2). Supplementary Figure S3 shows the proximity of the MAIA-derived PRL to the FPC in two cases with 0.1° and 1.2° AMC–FPC offsets.

Impact of Foveal Location on Cone Mosaic Analysis

Cone mosaic analysis was available in 12 of 15 control subjects and 15 of 15 patients. In total, 24 ROIs were excluded due to poor quality ($n = 21$) or absence of cone mosaic within portions of the AO imaging area ($n = 3$). Multiple regression analysis revealed that the distance between the AMC and FPC was the most significant determinant of cone density and inter-cone distance measurements, after adjustment for age, sex, SE, AL, eccentricity, and disease status (Table 4). Pairwise analysis showed no significant differences in cone metrics among any of the corresponding ROIs between the AMC and the FPC referencing methods (Table 5, Fig. 6A, Supplementary Table S3).

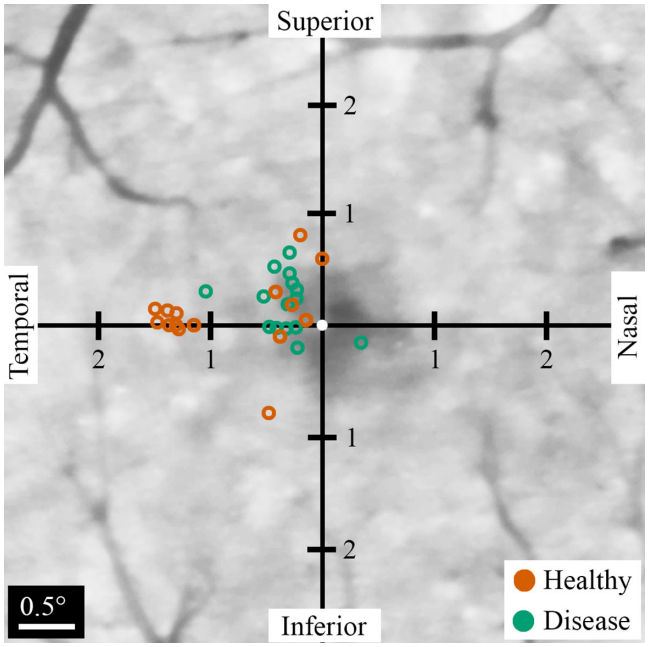

Figure 5. Location of the AMCs in relation to the FPCs (*white dot*) in healthy subjects (*orange*) and patients with RCD (*green*). Note that the temporal deviation of the AMC is more prominent in healthy subjects.

Table 3. Determinants of Horizontal Discordance Between the AMC and FPC

Factors	β Estimate	CI Lower	CI Upper	*P*
Intercept	11.29	–15.39	37.97	0.383
Age (y)	0.17	–0.01	0.04	0.122
Sex (male/female)	0.00	–0.94	0.94	0.998
BCEA 63% (deg^2)	–5.22	–14.31	3.87	0.241
BCEA 95% (deg^2)	1.70	–1.37	4.78	0.258
P1 (%)	0.2	–0.11	0.16	0.730
P2 (%)	–0.17	–0.51	0.17	0.307
BCVA (logMAR)	1.12	–1.65	3.90	0.403
MS (dB)	0.02	–0.03	0.06	0.486
Healthy/disease	–0.98	–1.76	–0.20	0.017

Discussion

The relationship between the PRL and anatomical foveal landmarks has been investigated using various devices and methods. Putnam and colleagues[19] for the first time reported a less than 50-µm (equivalent to approximately 0.15°) deviation of the PRL from the location of peak cone density, with no directional predominance, using the Rochester flood-illumination AO ophthalmoscope in three healthy subjects between the ages of 22 to 30 years. Wilk and colleagues[5] examined the relationship between the AOSLO-derived PRL

Table 4. Determinants of Cone Density and Inter-Cone Distance Adjusted for Age, Sex, Axial Length, Spherical Equivalent, Disease Status, and Eccentricity

Parameter	Factors (°)	β Estimate	CI		*P*
			Lower	Upper	
Cone density (cell/deg^2)	Rotation	2.6	–28.2	33.5	0.866
	x-Axis distance	272	173	371	<0.001
	y-Axis distance	259	113	406	0.001
	Overall distance	218	107	330	<0.001
Inter-cone distance (arcmin)	Rotation	0.02	–0.03	0.06	0.492
	x-Axis distance	0.28	0.15	0.40	<0.001
	y-Axis distance	0.21	0.45	0.91	0.028
	Overall distance	0.22	0.07	0.36	0.003

and anatomical foveal parameters, including the foveal avascular zone center, FPC, and locus of peak cone density. The mean distance between the PRL and FPC was 80 µm (range, 7.2–177), which is approximately equivalent to 0.27° (range, 0.02°–0.59°). More recently, Reiniger and colleagues[20] used an AOSLO camera in conjunction with a small flashing (3 Hz) light and reported a systematic nasosuperior offset of the PRL from the locus of peak cone density. They found an average of 5-arcmin distance, which was mirrored in the fellow eye. A similar distance without a consistent direction was reported by other authors.[21,22]

We reported a consistent temporal deviation of the AMC that was markedly greater than the PRL shift from the FPC reported previously. This difference can be explained by the different methods that were used. The AMC was determined using a commercial flood-illumination AO camera, which has a relatively low frame capture rate (10 frames per second) compared with AOSLO-based methods. For example, Reiniger et al.[20] and Bowers et al.[2] used AOSLO cameras that captured 30 and 960 frames per second, respectively. The AMC was derived from the average of the four separate (0,0) coordinates marked by the device using the raw image with the best image quality (according to the manufacturer). The (0,0) locus for each AO image is only one of many retinal loci used by the subject for gazing at the fixation target during the 4 seconds of AO image acquisition. In contrast, the PRL is estimated based on the center of all fixation points used during the entire duration of the MAIA 10-2 test; hence, it is not surprising that an AMC derived from AO image acquisition is different from the PRL derived from microperimetry. Another important difference is the choice of anatomical landmark. The location of the peak cone density that was used by most previous reports may not coincide with other anatomical landmarks, including FPC that was used in the present study.[19] Unlike the AMC, which is an estimation of the fixation point at the time of image acquisition that can vary widely, PRL and peak cone density loci have been shown to be less variable and usually located close to the FPC in healthy eyes. Thus, our findings suggest that the AMC may not correlate well with PRL or the location of peak cone density.

We recommend caution when comparing our findings with previous reports, as these results may differ with the use of a different AO camera, fixation target, software, and imaging protocol. More importantly, we analyzed only the right eyes; therefore, it is impossible to ascertain whether the observed temporal shift of the AMC in relation to the FPC was due to environmental or developmental factors. The location of fixation can be shifted through deliberate

Table 5. Average Cone Density Using the AMC and FPC as Reference at 2° and 4° Eccentricities Along Vertical and Horizontal Meridians

Group	Meridian	2° (Cells/deg^2)			4° (Cells/deg^2)		
		AMC	FPC	*P*	AMC	FPC	*P*
Healthy	Nasal	1702	1819	0.575	1733	1525	0.051
	Temporal	1881	1754	0.059	1289	1466	0.008
	P	0.059	0.695		0.003	0.594	
	Superior	1763	1865	0.071	1227	1233	0.875
	Inferior	1780	1754	0.695	1195	1212	0.424
	P	0.530	0.814		0.937	0.657	
	Mean	1785	1813	0.071	1353	1351	0.775
Disease	Nasal	1250	937	0.013	773	600	0.541
	Temporal	1547	1487	0.733	871	859	0.861
	P	0.030	0.016		0.155	0.060	0.424
	Superior	1168	1044	0.397	603	547	0.929
	Inferior	1165	1002	0.039	696	649	0.248
	P	0.778	0.388		0.239	0.169	
	Mean	1287	1130	0.013	737	665	0.223

Bonferroni correction of $\alpha = 0.05$ to 32 comparisons was set at 0.0016.

training, asymmetries in daily visual behavior (e.g., reading from left to right), or testing conditions (e.g., transient factors relating to participant attention or expectation). In such circumstances, we would expect to see a nasal (asymmetrical) shift of the fixation point in relation to the FPC in the left eye. If, however, the shift was due to developmental factors, we would expect a temporal (symmetrical) shift in the left eye. Without interocular data for comparison, we are unable to explore the root cause of this temporal deviation of the AMC.

Displacement of the AMC relative to the FPC has seldom been studied in generalized retinal dystrophies such as RCD, which retains good foveal function. In the present study, patients with RCD showed a significantly smaller AMC–FPC discordance compared with the healthy individuals. This difference was independent of potential confounding factors such as fixation parameters, visual acuity, and macular sensitivity. We propose that progressive centripetal photoreceptor degeneration may reduce the probability and distance range of perifoveal locations that are used for fixation and push the AMC toward the FPC. Although this speculation cannot be supported by our MAIA 10-2 fixation data, we hypothesize that patients with RCD may tend to use more central fixation loci, as these loci are farthest from the affected perifoveal retina and the transitional zone. Additionally,

Investigative Ophthalmology & Visual Science

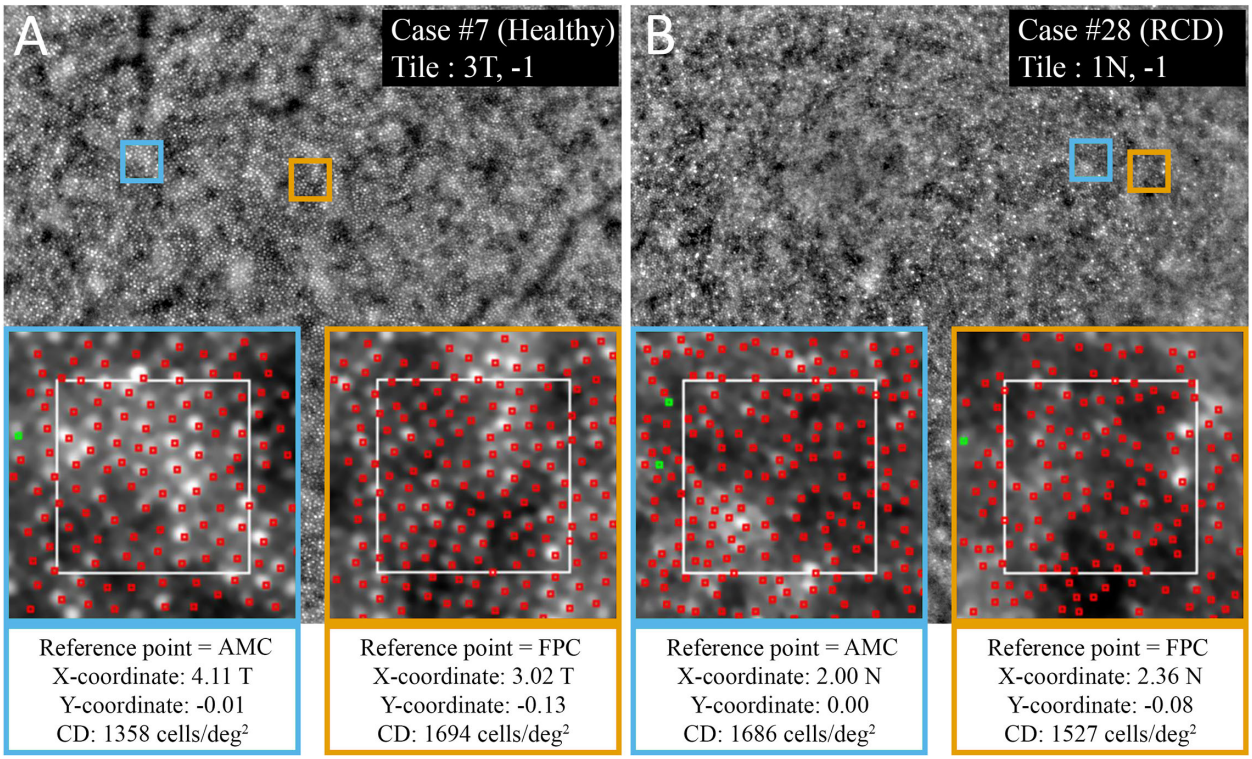

Figure 6. Examples of cone density (CD) analysis at temporal 4° in a healthy subject and nasal 2° in a patient with RCD using the AMC (*blue*) and FPC (*orange*) as reference points. (**A**) Using the AMC as a reference resulted in increased foveal distance and decreased CD at temporal 4°. (**B**) Using the FPC as a reference resulted in decreased foveal distance and increased CD. Note that, in cases with large discordance, using the AMC resulted in the nasal 2° ROI falling closer to the foveal center where the camera had limited resolution for visualizing cones. T, temporal; N, nasal; –, inferior.

compensatory hypersensitivity of the residual central foveal cones as a result of perifoveal cone loss in patients with RCD[23] may explain the dominance of central foveal fixation and deviation of the AMC toward the FPC. Increased visualization of foveal cones in flood-illumination AO imaging in patients with RCD has been reported in previous studies.[24,25] Although this phenomenon was attributed to the photoreceptor loss and increased cone spacing,[13,25] the underlying mechanism remains unexplained. Furthermore, the functional implications of increased cone visibility have not been explored. A comparison between the rod- and cone-specific residual visual fields and their correlation with the AMC–FPC discordance may further elucidate the underlying mechanism.

Several authors have used the PRL or AMC as the reference for retinal eccentricity and cone mosaic analysis.[12,26,27] However, this method has been questioned by other authors.[13,16] In addition to the offset from the anatomical center, intersession variations in AMC and PRL positions[28] may alter follow-up ROI localization and affect longitudinal analysis. Although our study did not reveal significant deviations in healthy subjects or patients with RCD with respect to the two types of reference chosen, the sample size may be too small to detect the small discrepancies from the shift in reference loci. The clinical significance of any differences in cone metrics arising from the use of alternative reference coordinates also must be evaluated in the context of inter-observer variability (4%)[10] and the test–retest variability in both healthy and diseased eyes.[13,23] We recommend careful alignment of the AO montage with a FPC-marked en face fundus image derived from a registered SD-OCT scan to ensure precise and reproducible localization of the eccentricities and ROIs. However, our data suggest that, in the absence of en face images to enable alignment of anatomical landmarks, a precisely determined AMC can be used as a reference for retinal eccentricity, without a significant impact on cone metric analysis outcomes.

The main limitation of our study was the lack of data on other fixation properties such as ocular dominance, eccentric fixation, and microtropia. This information may explain the deviation of the AMC from the FPC, at least in some cases. In addition, bilateral imaging along with determination of the ocular dominance may provide useful information regarding the symmetry and the impact of ocular dominance on AMC location in relation to the FPC. Localization of the PRL could be improved by using a higher quality MAIA sensitivity map on a fundus image. This was a significant limitation in our study, as precise alignment of the MAIA fundus image with the other imaging modalities was not feasible in all cases due to poor image quality related to over- or underexposure of the fundus image, defocus, and blurriness. Finally, the rtx1 AO machine that we used in the present study had not been calibrated by the manufacturer since initial installation. However, the optical misalignment between the fixation target and the coordinate displayed on the AO image is only up to 8 arcmin, which is insignificant compared to the disparity found between the AMC and FPC.

Investigative Ophthalmology & Visual Science

Conclusions

The AMC was located (on average) 0.85° temporal to the FPC in normal eyes but this did not result in a significant difference in cone mosaic measurements using the flood-illumination AO camera at the locations tested. The disparity between the AMC and FPC was smaller in the RCD patient cohort. These findings warrant further investigations using larger samples to clarify the relevance of the AMC–FPC disparity in cone mosaic measurement disagreement and its change in retinal pathologies.

Acknowledgments

The authors thank the participants, as well as Amanda Scurry and Jayme Glynn for their assistance in organizing the patient appointments for the clinical assessments.

Supported by grants from the Australian National Health and Medical Research Council (GNT1116360, GNT1188694, GNT1054712, and MRF1142962 to FKC); by the Australian Government Research Training Program Scholarship at The University of Western Australia (DR); and by the McCusker Charitable Foundation (FKC). The sponsor or funding organization had no role in the design or conduct of this research.

Disclosure: **D. Roshandel**, None; **D.M. Sampson**, None; **D.A. Mackey**, None; **F.K. Chen**, None

References

1. Gong Y, Chen LJ, Pang CP, Chen H. Ellipsoid zone optical intensity reduction as an early biomarker for retinitis pigmentosa. *Acta Ophthalmol.* 2021;99(2):e215–e221.
2. Bowers NR, Gautier J, Lin S, Roorda A. Fixational eye movements in passive versus active sustained fixation tasks. *J Vis.* 2021;21(11):16.
3. Castet E, Crossland M. Quantifying eye stability during a fixation task: a review of definitions and methods. *Seeing Perceiving.* 2012;25(5):449–469.
4. Molina-Martín A, Piñero DP, Pérez-Cambrodí RJ. Normal values for microperimetry with the MAIA microperimeter: sensitivity and fixation analysis in healthy adults and children. *Eur J Ophthalmol.* 2017;27(5):607–613.
5. Wilk MA, Dubis AM, Cooper RF, Summerfelt P, Dubra A, Carroll J. Assessing the spatial relationship between fixation and foveal specializations. *Vision Res.* 2017;132:53–61.
6. Steinman RM. Effect of target size, luminance, and color on monocular fixation. *J Opt Soc Am.* 1965;55(9):1158–1164.
7. Thaler L, Schütz AC, Goodale MA, Gegenfurtner KR. What is the best fixation target? The effect of target shape on stability of fixational eye movements. *Vision Res.* 2013;76:31–42.
8. McCamy MB, Najafian Jazi A, Otero-Millan J, Macknik SL, Martinez-Conde S. The effects of fixation target size and luminance on microsaccades and square-wave jerks. *PeerJ.* 2013;1:e9.
9. Wells-Gray EM, Choi SS, Bries A, Doble N. Variation in rod and cone density from the fovea to the mid-periphery in healthy human retinas using adaptive optics scanning laser ophthalmoscopy. *Eye (Lond).* 2016;30(8):1135–1143.
10. Legras R, Gaudric A, Woog K. Distribution of cone density, spacing and arrangement in adult healthy retinas with adaptive optics flood illumination. *PLoS One.* 2018;13(1):e0191141.
11. Lombardo M, Serrao S, Ducoli P, Lombardo G. Eccentricity dependent changes of density, spacing and packing arrangement of parafoveal cones. *Ophthalmic Physiol Opt.* 2013;33(4):516–526.
12. Feng S, Gale MJ, Fay JD, et al. Assessment of different sampling methods for measuring and representing macular cone density using flood-illuminated adaptive optics. *Invest Ophthalmol Vis Sci.* 2015;56(10):5751–5763.
13. Gale MJ, Harman GA, Chen J, Pennesi ME. Repeatability of adaptive optics automated cone measurements in subjects with retinitis pigmentosa and novel metrics for assessment of image quality. *Transl Vis Sci Technol.* 2019;8(3):17.
14. Strauss RW, Dubis AM, Cooper RF, et al. Retinal architecture in RGS9- and R9AP-associated retinal dysfunction (bradyopsia). *Am J Ophthalmol.* 2015;160(6):1269–1275.e1.
15. Woog K, Legras R. Visual resolution and cone spacing in the nasal and inferior retina. *Ophthalmic Physiol Opt.* 2018;38(1):66–75.
16. Chew AL, Sampson DM, Kashani I, Chen FK. Agreement in cone density derived from gaze-directed single images versus wide-field montage using adaptive optics flood illumination ophthalmoscopy. *Transl Vis Sci Technol.* 2017;6(6):9.
17. Sampson DM, Roshandel D, Chew AL, et al. Retinal differential light sensitivity variation across the macula in healthy subjects: importance of cone separation and loci eccentricity. *Transl Vis Sci Technol.* 2021;10(6):16.
18. Roshandel D, Thompson JA, Charng J, et al. Exploring microperimetry and autofluorescence endpoints for monitoring disease progression in *PRPF31*-associated retinopathy. *Ophthalmic Genet.* 2021;42(1):1–14.
19. Putnam NM, Hofer HJ, Doble N, Chen L, Carroll J, Williams DR. The locus of fixation and the foveal cone mosaic. *J Vis.* 2005;5(7):632–639.
20. Reiniger JL, Domdei N, Holz FG, Harmening WM. Human gaze is systematically offset from the center of cone topography. *Curr Biol.* 2021;31(18):4188–4193.e83.
21. Kilpeläinen M, Putnam NM, Ratnam K, Roorda A. The retinal and perceived locus of fixation in the human visual system. *J Vis.* 2021;21(11):1–14.
22. Li KY, Tiruveedhula P, Roorda A. Intersubject variability of foveal cone photoreceptor density in relation to eye length. *Invest Ophthalmol Vis Sci.* 2010;51(12):6858–6867.
23. Roshandel D, Heath Jeffery RC, Charng J, et al. Short-term parafoveal cone loss despite preserved ellipsoid zone in rod cone dystrophy. *Transl Vis Sci Technol.* 2021;10(14):11.
24. Duncan JL, Zhang Y, Gandhi J, et al. High-resolution imaging with adaptive optics in patients with inherited retinal degeneration. *Invest Ophthalmol Vis Sci.* 2007;48(7):3283–3291.
25. Gale MJ, Feng S, Titus HE, Smith TB, Pennesi ME. Interpretation of flood-illuminated adaptive optics images in subjects with retinitis pigmentosa. *Adv Exp Med Biol.* 2016;854:291–297.
26. Lombardo M, Lombardo G, Schiano Lomoriello D, Ducoli P, Stirpe M, Serrao S. Interocular symmetry of parafoveal photoreceptor cone density distribution. *Retina.* 2013;33(8):1640–1649.
27. Lombardo M, Serrao S, Lombardo G. Technical factors influencing cone packing density estimates in adaptive optics flood illuminated retinal images. *PLoS One.* 2014;9(9):e107402.
28. Molina-Martín A, Piñero DP, Pérez-Cambrodí RJ. Reliability and intersession agreement of microperimetric and fixation measurements obtained with a new microperimeter in normal eyes. *Curr Eye Res.* 2016;41(3):400–409.